CHEMISTRY
A EUROPEAN JOURNAL

DOI: 10.1002/chem.200500104

Low-Pressure Pyrolysis of tBu$_2$SO: Synthesis and IR Spectroscopic Detection of HSOH

Helmut Beckers,*[a] Simone Esser,[b] Thorsten Metzroth,[c] Markus Behnke,[b] Helge Willner,[a] Jürgen Gauss,*[c] and Josef Hahn*[b]

Abstract: Sulfenic acid (HSOH, **1**) has been synthesized in the gas-phase by low-pressure high-temperature (1150 °C) pyrolysis of di-*tert*-butyl sulfoxide (tBu$_2$SO, **2**) and characterized by means of matrix isolation and gas-phase IR spectroscopy. High-level coupled-cluster (CC) calculations (CCSD(T)/cc-pVTZ and CCSD(T)/cc-pVQZ) support the first identification of the gas-phase IR spectrum of **1** and enable its spectral characterization. Five of the six vibrational fundamentals of matrix-isolated **1** have been assigned, and its rotational-resolved gas-phase IR spectrum provides additional information on the O–H and S–H stretching fundamentals. Investigations of the pyrolysis reaction by mass spectrometry, matrix isolation, and gas-phase FT-IR spectroscopy reveal that, up to 500 °C, **2** decomposes selectively into *tert*-butylsulfenic acid, (tBuSOH, **3**), and 2-methylpropene. The formation of the isomeric sulfoxide (tBu(H)SO, **3a**) has been excluded. Transient **3** has been characterized by a comprehensive matrix and gas-phase vibrational IR study guided by the predicted vibrational spectrum calculated at the density functional theory (DFT) level (B3LYP/6-311+G(2d,p)). At higher temperatures, the intramolecular decomposition of **3**, monitored by matrix IR spectroscopy, yields short-lived **1** along with 2-methylpropene, but also H_2O, and most probably sulfur atoms. In addition, HSSOH (**6**), H_2, and S_2O are found among the final pyrolysis products observed at 1150 °C in the gas phase owing to competing intra- and intermolecular decomposition routes of **3**. The decomposition routes of the starting compound **2** and of the primary intermediate **3** are discussed on the basis of experimental results and a computational study performed at the B3LYP/6-311G* and second-order Møller–Plesset (MP2/6-311G* and RI-MP2/QZVPP) levels of theory.

Keywords: flash pyrolysis · gas-phase reactions · IR spectroscopy · matrix isolation · quantum chemical calculations

Introduction

HSOH (**1**), the elusive link between hydrogen peroxide (HOOH)[1] and disulfane (HSSH),[2] is alternatively named oxadisulfane or sulfenic acid, and is the first member of the series of oxygen-containing sulfur acids H_2SO_n (n = 1–4).[3] It has previously been obtained by low-pressure flash thermolysis of di-*tert*-butyl sulfoxide, tBu$_2$SO (**2**) according to Equation (1), and is characterized in the gas phase by mass spectrometry and its rotational spectra.[4]

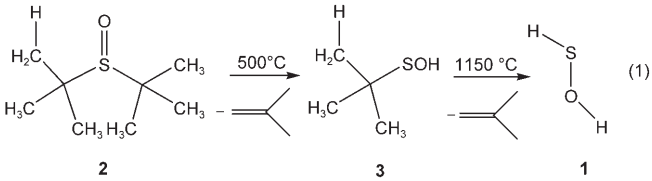

(1)

[2H/S/O] species are widely considered to play a crucial role in the atmospheric[5] and combustion chemistry of sulfur.[6] Despite numerous experimental[7] and theoretical investigations[8] that explore the reactions of hydrogen sul-

[a] Dr. H. Beckers, Prof. Dr. H. Willner
FB C, Anorganische Chemie
Bergische Universität Wuppertal
Gaußstrasse 20, 42097 Wuppertal (Germany)
Fax: (+49) 202-439-3035
E-mail: beckers@uni-wuppertal.de

[b] Dipl.-Chem. S. Esser, Dr. M. Behnke, Prof. Dr. J. Hahn
Institut für Anorganische Chemie, Universität zu Köln
Greinstrasse 6, 50939 Köln (Germany)
Fax: (+49) 221-470-4899
E-mail: hahn@uni-koeln.de

[c] Dipl.-Chem. T. Metzroth, Prof. Dr. J. Gauss
Institut für Physikalische Chemie, Universität Mainz
Jakob-Welder Weg 11, 55099 Mainz (Germany)
Fax: (+49) 6131-39-23859
E-mail: gauss@uni-mainz.de

fide (H_2S) with oxygen atoms, simple [2H/S/O] species still remained poorly characterized. First experimental evidence for the existence of **1** came from an IR spectroscopic investigation of the reaction of oxygen atoms with matrix-isolated hydrogen sulfide in solid argon.[9] More recently, gaseous **1** and H_2OS (**4**, dihydrogen thiooxonium ylide) have been generated from H_2S/N_2O and CS_2/H_2O mixtures, respectively, in neutralization–reionization mass spectrometric experiments.[10]

Persistent efforts made to synthesize sulfenyl halides (HSX, X = F,[11] Cl, Br[12]) and their parent acid **1**[4] in the last three decades have shown that flash pyrolysis of **2** [Eq. (1)] is obviously the first suitable route to provide sufficient quantities of one of these highly reactive species in the gas phase and is essential for a thorough structural and chemical characterization. Low-pressure flash pyrolysis of *tert*-butyl-alkyl sulfoxides [*t*Bu(R)SO] has been investigated by several groups in the past.[13] It was shown that pyrolysis of *t*Bu(R)SO yields transient alkylsulfenic acids RSOH (R = Me, *i*Pr, and, *t*Bu (**3**))[14] However, in these earlier studies, **1** has not been detected in the pyrolysis products of any of the investigated sulfoxides.

The reported synthesis of HSOH (**1**) by flash thermolysis of **2** has been assumed to proceed in two steps, and there is no doubt that the intermediate *t*BuSOH (**3**) is formed as a primary pyrolysis product.[4,14] The direct formation of **1** by thermal elimination of 2-methylpropene from **3** [Eq. (1)] requires a comparatively strained four-membered transition state, although elimination of 2-methylpropene from **3** through a competing five-membered transition state cannot be ruled out. This route would not lead directly to HSOH, but would produce transient H_2OS (**4**) [Eq. (2)] instead. Compound **4** has been found experimentally to be a viable molecule in the gas phase[10] and is predicted by quantum chemical calculations to be higher in energy than the unbranched isomer HSOH by 166 kJ mol^{-1}.[8b] At pyrolytic temperatures it might decompose rapidly into H_2O and sulfur atoms.

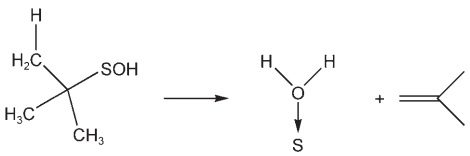

3 4 (2)

Davies et al.[14b] claimed that transient *tert*-butylsulfenic acid could, in principle, exist in two tautomeric forms: the O-protonated sulfenic acid **3** and its *S*-protonated isomer, *tert*-butyl hydrogen sulfoxide, *t*Bu(H)SO (**3a**). From the IR absorption spectra of products obtained by flash pyrolysis of **2**, deposited on a NaCl window at −196 °C, they inferred that some transient *S*-protonated tautomer **3a** was formed, whereas **3** clearly represented the favored product.

*t*Bu(H)SO (**3a**) appears to be properly suited to furnish **1** by elimination of 2-methylpropene through a less-strained five-membered cyclic transition state [Eq. (3)], hence **3a** may appear to be the crucial intermediate furnishing **1** by flash pyrolysis of **2**.

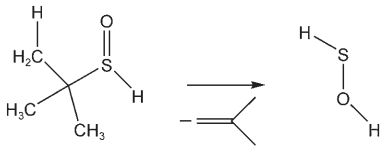

3a 1 (3)

Thus, the principal objectives of the present study are: i) to explore the decomposition pathways of the starting compound **2** and those of the potential HSOH precursors *t*BuSOH (**3**) and *t*Bu(H)SO (**3a**) experimentally by mass spectrometry as well as gas-phase and matrix FT-IR spectroscopy, and computationally at the density-functional theory (DFT) as well as second-order Møller-Plesset (MP2) levels of theory, and ii) to identify highly reactive **1** for the first time in its gas-phase IR spectrum.

Results and Discussion

Quantum chemical calculations

Formation of HSOH (1): The formation of **1** by pyrolysis of **2** is studied quantum chemically by determining the equilibrium and transition-state geometries of the species and intermediates involved. The calculations have been carried out with i) second-order Møller–Plesset perturbation theory (MP2)[15] and ii) density-functional theory (DFT),[16] employing the B3LYP hybrid functional.[17] The simultaneous use of two conceptionally different quantum chemical approaches turns out to be advantageous because it allows a check of the reliability of the computational results.

Calculations were initially performed at both DFT and MP2 level with a 6-311G* basis set[18] with a polarized valence triple-zeta quality. In a second step, improved energies were obtained at the MP2 level (within the resolution-of-identity (RI) MP2 approximation[19] with the MP2/6-311G* optimized geometries) using a larger doubly-polarized valence quadruple-zeta set (QZVPP[20]). As usual, all computed stationary points were characterized by evaluating the corresponding harmonic force fields. Furthermore, to ensure that the computed transition states properly connect educts and products, intrinsic reaction coordinate (IRC)[21] calculations were performed for all reaction steps under consideration. The computed harmonic frequencies are used to determine zero-point vibrational energy corrections to the reaction energies and to convert the energies to enthalpies and free enthalpies. Temperature corrections were evaluated with the standard harmonic-oscillator rigid-rotator approximation.

Figure 1 gives an overview over the computed structures within the proposed reaction schemes. Computed free en-

thalpies of reaction and activation barriers for the actual experimental conditions (723 K for the initial step in the pyrolysis reaction, and 1473 K for the second step, each at 10 Pa) are given in Figures 2–4, and the free enthalpy surface is shown in Figure 5.

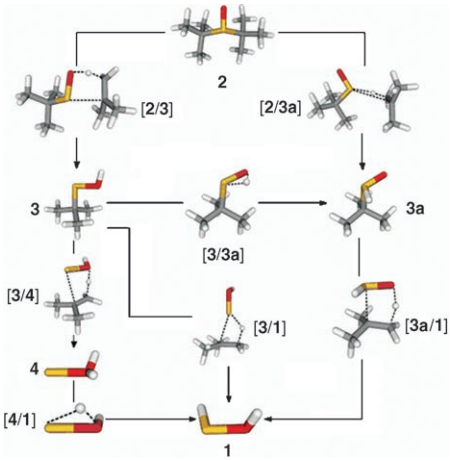

Figure 1. Computed equilibrium and transition state (TS) structures (MP2/6-311G*) for possible reaction steps in the formation of HSOH (**1**). Transition states are denoted in brackets.

Comparison of the MP2 and DFT results reveals differences of $\approx 80\,kJ\,mol^{-1}$ for the initial fragmentation of **2** and $\approx 40\,kJ\,mol^{-1}$ for the fragmentation of *t*BuSOH (**3**). Because these deviations are comparatively large, the implemented methods (DFT-B3LYP/6-311G*, MP2/6-311G* and RI-MP2/QZVPP) have been calibrated for the energy difference between HSOH and H_2SO with reliable coupled-cluster data obtained at the CCSD(T)/cc-pCVQZ level. As only the RI-MP2/QZVPP numbers are in satisfactory agreement with these high-level results ($-72\,kJ\,mol^{-1}$ CCSD(T)/cc-pCVQZ, $-70\,kJ\,mol^{-1}$ RI-MP2/QZVPP, $-116\,kJ\,mol^{-1}$ MP2/6-311G*, $-106\,kJ\,mol^{-1}$ DFT B3LYP/6-311G*) we will discuss only the RI-MP2/QZVPP data in the following (the corresponding DFT/6-311G* and MP2/6-311G* results can be obtained from the authors). Furthermore, it should be emphasized that our intent is not so much to yield highly accurate predictions for the reaction energies and enthalpies, but rather to shed light on the preferred reaction mechanisms so that even less accurate results obtained at a lower computational level are adequate for this purpose.

Figure 2 reveals that elimination of 2-methylpropene is endergonic for all processes at 0 K. At 773 K (Figure 3), both initial fragmentation steps are found to be exergonic with a significant preference (based on ΔG and $\Delta G^{\neq}$) for the formation of *t*BuSOH (**3**, Figure 3). However, the isomerization of **3** to *t*Bu(H)SO (**3a**) is endergonic at this temperature and, in particular, has a high activation barrier of $219\,kJ\,mol^{-1}$. According to the computational results, it is thus unlikely that **3a** is formed in the fragmentation of **2** at 773 K. Whereas RI-MP2 results at this temperature indicate that the elimination of a second 2-methylpropene from **3** to form H_2OS (**4**) is endergonic ($\Delta G = 90\,kJ\,mol^{-1}$), the reaction to **1** is exergonic ($\Delta G = -80\,kJ\,mol^{-1}$). Both fragmentations show high enthalpies of activation ($\Delta G^{\neq}$(**1**) = $205\,kJ\,mol^{-1}$; $\Delta G^{\neq}$(**4**) = $254\,kJ\,mol^{-1}$). These comparatively large barriers impede a second 2-methylpropene abstraction to form **1** at that temperature. These findings are consistent with experimental results, as neither **4** nor **1** are found under these conditions.

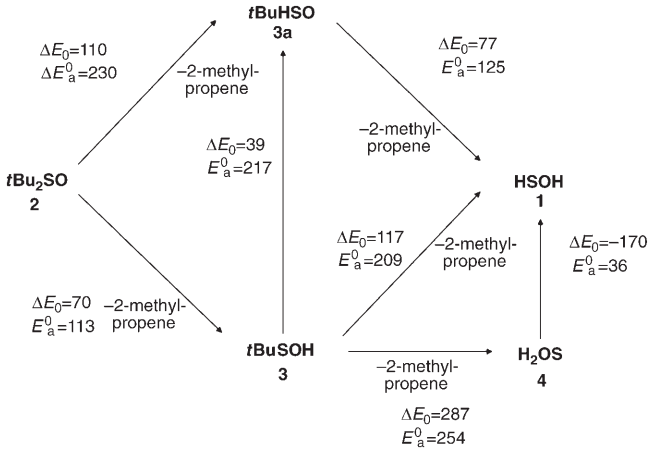

Figure 2. Possible reaction paths for the formation of HSOH (**1**); reaction energies ΔE_0 [$kJ\,mol^{-1}$] and activation barriers E_a^0 at 0 K [$kJ\,mol^{-1}$] at the RI-MP2/QZVPP level.

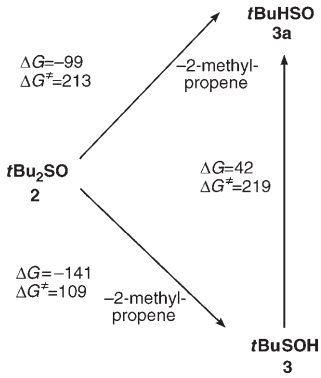

Figure 3. Reaction free enthalpies ΔG and free enthalpies of activation $\Delta G^{\neq}$ [$kJ\,mol^{-1}$] at 773 K and 10 Pa for the first fragmentation of *t*Bu_2SO (**2**) and the isomerization of *t*BuSOH (**3**) at the RI-MP2/QZVPP level.

The free enthalpy surface shown in Figure 5 reveals that the fragmentation of the primary pyrolysis product *t*BuSOH (**3**) leading to either **1** or **4** is possible (for numerical values, see Figure 4) and that it is probable that both processes take place simultaneously at 1473 K. Compound **4** can then rearrange to **1** ($\Delta G^{\neq} = 43\,kJ\,mol^{-1}$) or decompose to H_2O and S(^{1}D) ($\Delta G = -176\,kJ\,mol^{-1}$; sulfur calculated with UMP2 in its ^{3}P state and corrected by experimental S(^{3}P) to S(^{1}D) value of $110\,kJ\,mol^{-1}$;[22] $\Delta G^{\neq}$ values cannot be estimated easily).

Overall, it can be concluded that our computational results are in satisfactory agreement with the experimental

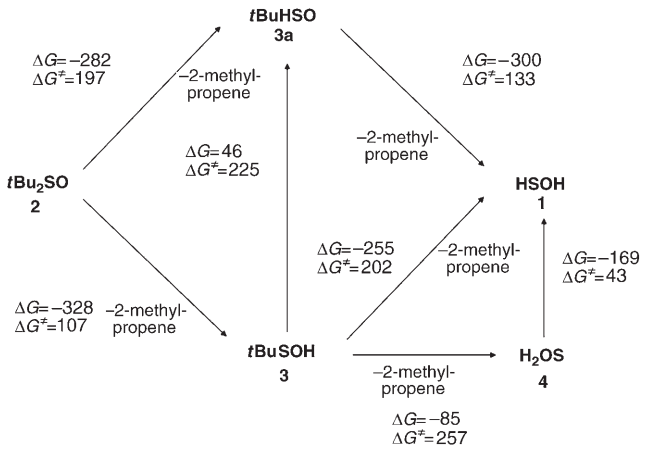

Figure 4. Possible reaction paths for the formation of HSOH (**1**); reaction free enthalpies ΔG and free enthalpies of activation $\Delta G^{\neq}$ [kJ mol^{-1}] at 1473 K and 10 Pa at the RI-MP2/QZVPP level.

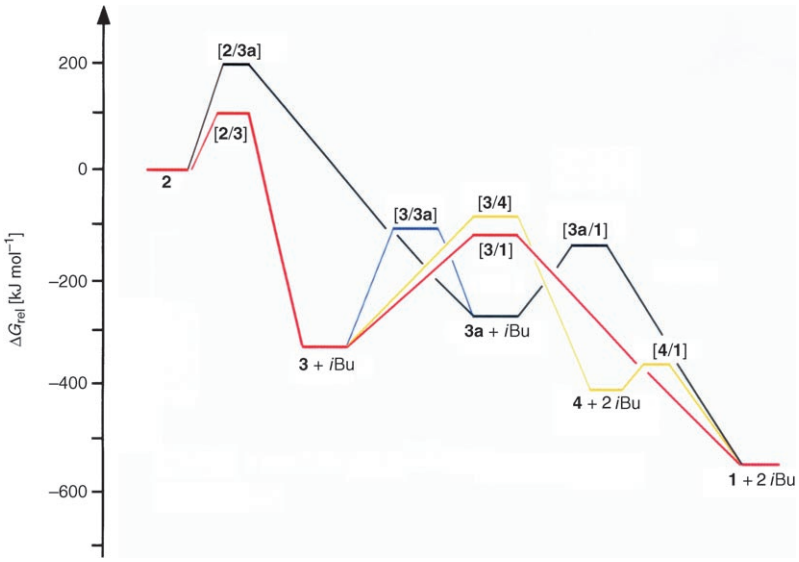

Figure 5. Free enthalpy surface at 1473 K and 10 Pa (RI-MP2 results). For notation and structures see Figure 1, iBu = 2-methylpropene.

findings, namely, that at the lower temperature (773 K) only one molecule of 2-methylpropene is eliminated from tBu$_2$SO (**2**), while fragmentation of a second 2-methylpropene proceeds solely at higher temperatures. Furthermore, the computational data indicate that **3a** probably plays a negligible role in the thermolysis of **2**, in contrast to previous postulations.[14b]

IR spectroscopic identification of HSOH (1): To assist in the IR spectroscopic identification of **1**, the equilibrium geometry as well as the corresponding vibrational frequencies of **1** were computed with a high-level treatment of electron correlation, namely, coupled-cluster (CC) theory. Calculations were performed at the CC singles and doubles (CCSD) level augmented by a perturbative treatment of triple excitations (CCSD(T)[29]) by means of analytical second derivative techniques[24] together with Dunning's correlation-consistent polarized valence-zeta sets, (cc-pVTZ[25] and cc-pVQZ).[25] Additional calculations were carried out at the B3LYP level with the 6-311+G(2d,p)[18,26] basis sets.

Whereas in the CC calculations, anharmonic contributions to the vibrational frequencies of the fundamentals were explicitly computed by means of a perturbation-theory approach[28] based on cubic and semidiagonal quartic force fields (computed at the CCSD(T)/cc-pVTZ level), the DFT harmonic frequencies were adjusted for anharmonic effects by means of a scaling factor of 0.9614, as advocated in ref. [28]. To verify the DFT results, calculations with the larger 6-311+G(2d,p) basis sets were performed in addition to 6-311G* calculations.

The results obtained for the vibrational frequencies of **1** are listed in Table 1. There is good agreement between the results obtained with the different methods and, in particular, the differences between the CCSD(T)/cc-pVTZ and CCSD(T)/cc-pVQZ results are comparatively small, indicating that remaining basis-set effects are more or less negligible. Anharmonic corrections to the vibrational frequencies amount to as much as 200 cm^{-1} for the O–H and S–H stretching frequencies, while for the other (low-frequency) modes the effects of less than 10 cm^{-1} are significantly smaller and less essential. Interestingly, scaling of the DFT results largely recovers the anharmonic contributions and leads to a good agreement with the more theoretically sound CC data.

Mass spectrometric analysis of flash pyrolysis products

Electron impact ionization (EI) mass spectra of tBu$_2$SO (**2**) measured at room temperature and those of the pyrolysis products obtained at a pyrolytic temperature of 1100 °C have already been discussed in the preceding paper.[4] Figure 6 displays an extended view of the thermal evolution of selected pyrolysis products monitored by mass spectrometry. Obviously, **2** decomposes rapidly above 200 °C, indicated by a decrease of the intensity of its $[M]^{+\cdot}$ signal at m/z 162. As expected for the thermal elimination of 2-methylpropene (m/z 56) from **2** [Eq. (1)], the drop in intensity of the signal at m/z 162 is mirrored by a rise in intensity of the signal at m/z 56. However, the $[M]^{+\cdot}$ ions of the two primary pyrolysis products, $[C_4H_8]^{+\cdot}$ at m/z 56 and $[C_4H_{10}SO]^{+\cdot}$ at m/z 106, cannot be distinguished from analogous fragment ions of $[t\text{Bu}_2\text{SO}]^{+\cdot}$. On the other hand, above 500 °C, a very low intensity of the $[M]^{+\cdot}$ peak at m/z 162 indicates nearly quantitative decomposition of **2** and thus the comparatively high intensity at m/z 106 can

Table 1. Calculated and experimental matrix IR and gas-phase IR vibrational wavenumbers of HSOH (**1**).[a]

	B3LYP/6-311+G(2d,p)	CCSD(T)/cc-pVQZ[c]		CCSD(T)/cc-pVTZ	Gas phase	Ar matrix	
	scaled harmonic[b]	harmonic	anharmonic	anharmonic	this work	this work	ref. [9]
ν(OH)	3647.1 (84)	3847.7 (92)	3657.2	3646.5	3625.6	3608.3(43)	3606.0[d](26)
ν(SH)	2504.1 (14)	2647.9 (22)	2536.9	2533.3	2538	2550.1 (8)	
δ(SOH)	1151.8 (43)	1221.9 (54)	1188.1	1183.5		1175.7(53)	1177 (56)
δ(OSH)	971.8 (2)	1027.8 (3)	1004.6	1006.6			
ν(SO)	706.3 (64)	776.9 (65)	756.7	764.4		762.5(103)	763 (100)
τ(HOSH)	457.9(100)	486.9(100)	451.7	448.1		445.3 (54)	444.8 (44)

[a] Relative intensities in parentheses. [b] Scaling factor of 0.9614 was used, see ref. [28]. [c] Anharmonic corrections taken from CCSD(T)/cc-pVTZ calculation. [d] Band was attributed to HOOH in ref. [9] and has now been reassigned to the O–H stretch of **1**.

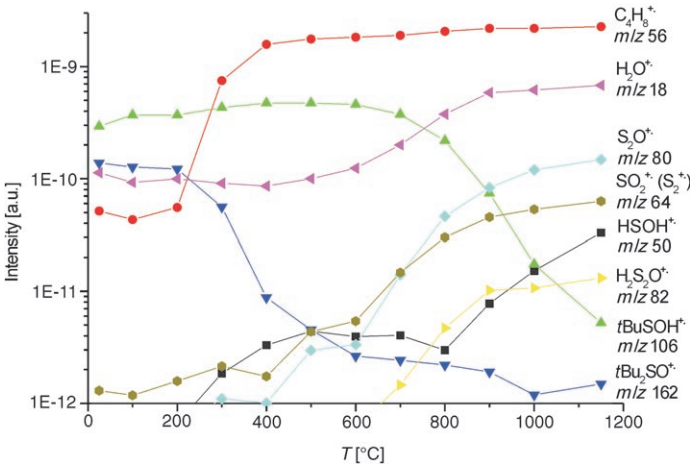

Figure 6. Thermal evolution of the pyrolysis products of tBu$_2$SO (**2**) in the temperature range between 25 and 1150 °C monitored by mass spectrometry (quadrupole RGA, EI 20 eV, enclosed ion source, 0.1 Pa).

only be explained by direct ionization of the primary pyrolysis product tBuSOH (**3**).

The mass spectrometric instrumentation does not allow differentiation between **3** and its constitutional isomer tBu(H)SO (**3a**). Nevertheless, at 500 °C, the formation of **3a** can be ruled out on the basis of the corresponding thermodynamic data (Figure 3) and the IR spectra of the matrix-isolated pyrolysis products obtained at that temperature (see below).

However, since intermediate formation of (**3a**) by elimination of 2-methylpropene form **2** cannot be excluded at higher pyrolytic temperatures, we carried out two-step pyrolysis experiments at 500 °C (nearly quantitative decomposition of **2** into 2-methylpropene and **3**) followed by pyrolysis of the primary products at 1150 °C. We observed that the mass spectra of this two-step pyrolysis and of a single-step pyrolysis at 1150 °C do not show any significant differences. Hence, the final pyrolysis products obtained at 1150 °C are assumed to evolve solely from the primary product **3**.

As can be concluded from the mass spectra (Figure 6), the decomposition of **2** is quite selective up to 500 °C because **3** and isobutene represent the only pyrolysis products (the intensity of the peak at m/z 18 corresponds to the background water signal). In contrast, pyrolysis of the primary product **3**, which starts above 500 °C, is less selective because, in addition to 2-methylpropene and small amounts of HSOH (**1**), several supplementary products emerge. According to Figure 6, these are S_2O, SO_2 (and/or S_2), H_2O (indicated by the increased intensity of the signal at m/z 18), and possibly HSSOH. The formation of the latter molecule is presumed because the peak at m/z 82 is always slightly higher than that expected for the isotopomer $S^{34}SO$. Additionally, as previously reported[4], H_2 and H_2S are also present in the pyrolysis products. However, because we do not detect H_2S in the IR spectra of the present study we cannot exclude that its mass spectroscopic detection originates from hydrogenation of sulfur in the ion source. We assume that the formation of HSSOH, S_2O, and some of the H_2O molecules can be traced back to the well-known condensation reaction of **3**[13,14] [Eq. (4)] and the subsequent decomposition of the condensation product according to Equation (5).

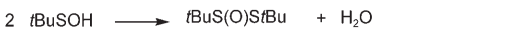

(4)

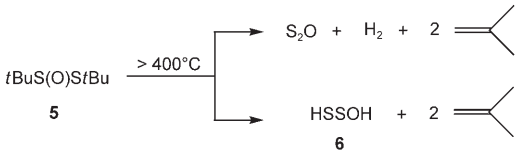

(5)

Previous investigations[14a] have shown that the pyrolysis of tBuS(O)StBu (**5**) furnished 2-methylpropene as well as S_2O and short-lived HSSOH (**6**) [Eq. (5)]. Thus, the condensation reaction [Eq. (4)] most probably competes with the desired formation of **1** [Eq. (1)], and yields the pyrolysis products H_2O, S_2O, HSSOH, and H_2. Previous studies[29] prove that S_2O decomposes to sulfur and SO_2. This decomposition reaction is the source of the SO_2 formed in our experiments.

Based on the proposed formation of **1** by thermal elimination of 2-methylpropene from **3**, one expects an increasing amount of $[HSOH]^{+\cdot}$ (m/z 50) as the signal associated with $[t$BuSOH$]^{+\cdot}$ (m/z 106) decreases on heating beyond 700 °C (Figure 6). Instead of this, the signal at m/z 50 slowly grows as the pyrolytic temperature is raised from 200 to 600 °C and slightly decreases on further heating up to 800 °C.

Above 800 up to 1150 °C, the intensity rises significantly. In the low temperature range from 200 to 600 °C, it appears that secondary fragmentation of the molecular ion $[t\text{BuSOH}]^{+\cdot}$ (m/z 106) [Eq. (6)] contributes to the signal at m/z 50, whereas the large increase of the signal intensity above 800 °C indicates the ionization of molecular **1**, which prevails at higher temperatures.

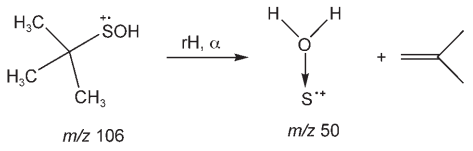

m/z 106 m/z 50 (6)

Even at 1150 °C, when the concentration of **3** is very low, the $[\text{HSOH}]^{+\cdot}$ signal (m/z 50) remains weaker than the $[M]^+$ signal of S_2O. As has been suggested before,[4] this can most probably be explained by condensation and subsequent decomposition reactions of **1**, which, by analogy with Equations (4) and (5), produce S_2O and thus contribute to the large increase of the signal at m/z 80 observed at temperatures above 700 °C.

Investigation of matrix-isolated pyrolysis products

The matrix-isolation experiments were carried out to obtain further information on the mechanism of the pyrolysis reaction. Gaseous **2**, diluted by a stream of argon (≈1:1000), is forced through a heated pipe with a corundum (Al_2O_3) nozzle prior to deposition on the matrix support at ≈15 K. Higher temperatures were needed for the pyrolytic process owing to the much shorter contact times in the hot zone than those employed in the mass spectrometric study. The pyrolysis temperatures were not measured directly, but were adjusted according to the progress of the decomposition reaction monitored by IR spectroscopy. The spectrum of the primary products, obtained after **2** had almost completely decomposed, is displayed in the upper traces of Figure 7 [a) 400–1800 cm^{-1}, b) 2500–3900 cm^{-1}], and the spectrum of the final pyrolysis products (complete decomposition of tBuSOH (**3**)) is shown in the lower traces.

IR spectrum of primary pyrolysis products: Part of the IR bands shown in Figure 7 occurs in both the upper and the lower traces. According to reference spectra recorded on authentic matrix-isolated samples of 2-methylpropene and water, almost all of them are associated with these two molecules. Some of the bands belonging to water are indicated in Figure 7. They show a noticeable increase in intensity at elevated pyrolysis temperatures and a decrease at lower temperatures. Thus, in agreement with the mass spectrometric study, the formation of water by the pyrolysis reaction is confirmed. The complexity of the IR spectra recorded on matrix-isolated water is attributed to i) rotational fine splitting (water monomers),[30a,b] ii) bands associated with the dimer and multimers of H_2O,[30c] and iii) fundamental bands of matrix-isolated complexes of water with other species.[30d]

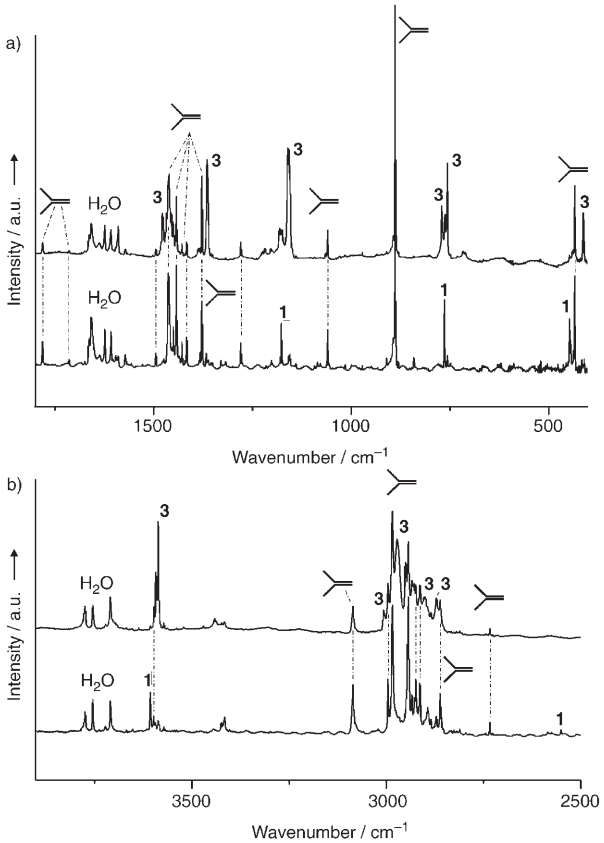

Figure 7. Argon-matrix IR spectra over the spectral regions a) 400–1800 cm^{-1} and b) 2500–3900 cm^{-1} of the deposit obtained by low-pressure pyrolysis of tBu$_2$SO (**2**) at two different pyrolytic temperatures. Upper trace: after complete decomposition of **2**. Lower trace: at higher temperatures. Bands arising in both spectra are attributed to the byproducts water and 2-methylpropene, as indicated. Absorptions of tBuSOH (**3**, upper traces) and HSOH (**1**, lower traces) are labeled.

IR absorptions of the bands found in the upper traces (primary products) but not in the lower traces of Figure 7 are collected in Table 2 and are compared to vibrational wavenumbers of **3** calculated at the B3LYP/6-311+G(2d,p) level of theory. The agreement between the experimental frequencies and those calculated for **3** is conclusive. For comparison, selected band positions obtained from our gas-phase experiments (see below) have been included in Table 2. In addition to the characteristic bands, associated with the tBu moiety, the gas-phase spectrum of **3**[14a], recorded from 400 to 4000 cm^{-1}, reveals four strong bands at 3609 (ν(OH)), 758 (ν(SO)), 1155 (δ(HOS)), and 418 cm^{-1} (δ(OSC)/τ(HOSC)). Close to these gas-phase values, at least three bands occurred in the IR matrix spectrum that are attributed to site splitting of matrix-isolated **3** species. Thus, almost all transitions observed in the upper traces of Figure 7, except those from water and 2-methylpropene, can be attributed to transient **3** and are assigned accordingly. Apparently, **3** is formed selectively by flash pyrolysis of **2** ac-

Table 2. Matrix- and gas-phase band positions and calculated vibrational wavenumbers in the 400–4000 cm^{-1} spectral range of *t*BuSOH (**3**) obtained by pyrolysis of tBu_2SO (**2**).

Ar matrix[a]	Gas phase[a]	B3LYP/6-311+G(2d,p) scaled by 0.9614[b,c]	Assignment[d]
3593.3 (m)			
3588 (s)	3609 (s)	3645.4 (68)	ν(OH)
3006.3 (m)			
		2988.2 (19)	
2975 (s, sh)		2978.7 (23)	
2972.1 (s)	2972[e] (s)	2972.3 (16)	ν_{as} (CH_3)
2968 (s, sh)	2967[e] (s)	2966 (37)	
		2963.1 (3)	
2950 (m)	2955[e] (m, sh)	2955.6 (13)	
2902.6 (m)		2908.2 (30)	ν_s (CH_3)
2899.2 (m)	2880[e] (m, br)	2903 (29)	
2870.8 (m)		2898.6 (22)	
2293.6 (w)			
2289 (w)	2292.5 (w)		$2\times\delta$(HOS)
1482.7 (w, sh)			
1477.6 (m)	1471[e] (m, br)	1460 (10)	δ_{as} (CH_3)
1467.6 (m)			
1460.8[e] (m, sh)		1443.9 (9)	
1455.1 (m)		1440.6 (9)	δ_{as} (CH_3)
		1431.9 (1)	
1387 (w)		1371.4 (1)	
1365.2 (s)	1368[e] (m)	1345.6 (11)	δ_s (CH_3)
1362.2 (m, sh)	1361 (m, sh)	1343.4 (10)	
1217 (w, br)	1217 (w)	1194 (2)	
1202.5 (w, br)		1188.5 (3)	ρ(CH_3)
1180.2 (m)	1181 (m)	1151.6 (34)	
1174.2 (m)			
1159.6 (s)			
1156.3 (s)	1155 (s)	1125.7 (42)	δ(HOS)
1154 (s)			
1064 (w)			
769.3 (s)			
767.3 (sh)			
761.1 (s)	758 (vs)	702.4 (79)	ν(SO)
755 (s)			
		420 (3)	$\delta(CC_3)$
410.4 (s)	418 (m)	402.6 (49)	τ(HOSC)/δ(OSC)
409 (m, sh)			

[a] Relative intensities: weak (w), medium (m), strong (s), very strong (vs), shoulder (sh), broad (br). [b] Relative intensities (1–79) in parentheses. [c] Scaling, see ref. [28]. [d] Vibrational modes: deformation (δ), stretching (ν), rocking (ρ), and torsion (τ). [e] Bands contributed by 2-methylpropene may interfere with those contributed by the *t*Bu moiety of **3**.

cording to Equation (1), and the predicted thermodynamic data are presented in Figure 3.

Sulfenic acids (RSOH) encumbered with comparatively bulky substituents, R = *t*Bu[14b] and 1,3,6-trimethyllumazine,[31] have been claimed to exist in two tautomeric forms, O- and S-protonated, similar to **3** and **3a**. The existence of the S-protonated isomers (R(H)SO), in the solid state at least, have solely been inferred from the presence of weak IR bands observed at 2600 and 2500 cm^{-1}, respectively, which have erroneously been assigned to S–H stretching fundamentals. Contrary to these assignments, the IR spectrum of *t*Bu(H)SO (**3a**), calculated at the B3LYP/6-311+G(2d,p) level, reveals prominent spectral features at $\tilde{\nu}$ = 2253 and 1012 cm^{-1} (scaling factor = 0.9614)[28] that are associated with strong S–H and S–O stretching vibrations, respectively, apart from much weaker fundamentals of the *t*Bu moiety. Obviously, the S–H stretch of **3a** is predicted to be strong and to appear at an exceptionally low frequency. However, an anomalously low frequency for elemental hydrogen stretching vibrations with adjacent oxo substituents has some precedents in the PH and NH stretching fundamentals of HPO[32] and HNO.[33]

A search for spectral features originating from **3a** in the matrix spectra of the primary pyrolysis products (upper traces of Figure 7) remains fruitless. Close to the predicted S–H stretching frequency of **3a** (2253 cm^{-1}), two weak lines appeared in the matrix spectra at $\tilde{\nu}$ = 2290 cm^{-1}, that correspond to a weak band in the gas-phase spectrum centered at 2292.5 cm^{-1}. However, these features are assigned to the first overtone of the strong HOS deformation of **3** located at 1155 cm^{-1}. The strong δ(HOS) fundamentals that are conspicuous in the gas-phase IR spectra of various sulfenic acids (RSOH, R = Me, *i*Pr, *t*Bu,[14a] and vinyl[34]) at $\approx$1155 cm^{-1} are always found to be accompanied by their first overtone. The latter band displays an analogous dependence of its wavenumber on the nature of the substituent R, as observed for the fundamental band.[34b] The absence of any detectable S–H fundamental bands from **3a** in the experimental spectra is at variance with the previous work of Davies et al.,[14b] but fully consistent with the predicted, much higher transition-state energy separating **3a** from **2** compared to that leading to the observed primary pyrolysis product **3** (Figure 5).

IR spectrum of the final pyrolysis products: In the matrix IR spectra of the pyrolysis products obtained at the highest temperatures (lower traces of Figure 7), at least five new absorptions at $\tilde{\nu}$ = 444.8, 762.5, 1175.7, 2550.1, and 3608.3 cm^{-1} appeared that are assigned to **1**. This assignment is based on the following findings:

1) The relative intensities of the five absorptions remain constant within experimental error at different pyrolysis temperatures. Owing to their uniform thermal behavior,

these bands are attributed to one single molecular species.

2) The four strongest absorptions under consideration have previously been observed by Smardzewski and Lin,[9] who explored the reaction between ground-state oxygen atoms O (^{3}P) and matrix-isolated hydrogen sulfide, H_2S. However, the present results as well as the quantum chemical calculations do not support the original assignment of a band at $\tilde{\nu} = 3425\,cm^{-1}$ to the O–H stretch of **1**. More consistent and in better agreement with the theoretical results (ν(calculated O–H stretch) = 3646.5 cm^{-1}, Table 1) is the assignment of this mode to the band at 3608.3 cm^{-1}, which was also detected (3606.0 cm^{-1}) by Smardzewski and Lin.[9] The weak band at 3425 cm^{-1} (erroneously assigned to HSOH in reference [9]) is also present in our spectrum (Figure 7); however, it does not experience the thermal behavior of the bands attributed to **1**. Thus, the present work verifies the first detection of **1** by Smardzewski and Lin,[9] but corrects their assignment of the O–H stretching vibration.
3) Both the experimental wavenumbers of **1** and the relative intensities are in good agreement with those predicted by quantum chemical calculations (Table 1).
4) Finally, the assigned fundamentals of **1** are comparable to the four strongest transitions observed for the HOSC moiety of **3** (Table 2). Furthermore, in agreement with the mass relations of F, OH, and Cl, the S–O stretch of **1** at 763 cm^{-1} is observed at slightly higher wavelengths than the O–Cl stretching frequency of Ar-matrix-isolated HOCl (728 cm^{-1}),[35] but at lower wavelengths than the S–F stretch of the closely related molecule HSF (787 cm^{-1}).[11c]

Reliable references confirming the position of the S–H stretch of **1** at 2550 cm^{-1} are difficult to find owing to the low intensity of this vibration and to the lack of synthetic routes to closely related molecules, such as sulfenyl halides (HSX, X = F,[11] Cl, Br[12]). Fortunately, in the spectral region predicted for this fundamental band, only the 2550 cm^{-1} band exhibits the expected thermal behavior. The assignment of the remaining unobserved absorption of **1**, the HSO bend, is impeded by its low intensity (for intensity predictions, see Table 1).

The experiments carried out at different temperatures revealed a comparatively high thermal stability of HSOH. Thermal decomposition of **1**, indicated by a decrease of its bands compared with selected absorptions of 2-methylpropene, is only observed at the highest temperatures employed. Nevertheless, no additional features emerge from the decomposition of **1**. Thus, at elevated temperatures, **1** appears to decompose into H_2O and sulfur atoms rather than SO and molecular hydrogen. A weak absorption found at 1138.5 cm^{-1} (lower trace in Figure 7a) may be associated with the absorption band of SO isolated in solid Ar previously reported to appear at 1136.9 cm^{-1}.[36] However, this absorption remains almost constant in intensity as the lines attributed to **1** decreased on heating beyond 1200 °C. This thermal behavior does not agree with a possible assignment to an SO band. Thus, the formation of SO in the pyrolysis reaction of **2** can be excluded.

IR spectra of gaseous pyrolysis products

The matrix-isolation experiments described above suggest a promising simple thermal decomposition of **3** to produce **1** and H_2O simultaneously along with 2-methylpropene by competing unimolecular routes. In contrast to this, the mass spectrometric analysis of gaseous pyrolysis products (vide supra) revealed a much more complex thermal behavior of **3**.

In order to verify our mass spectrometric results and to unambiguously ascertain the existence and the relative amount of HSOH (**1**) in the gas phase, we recorded rotationally resolved gas-phase FT-IR spectra of the pyrolysis products of **2** in a flow system equipped with a White-type long-path absorption cell. The total path length was adjusted to 40 m. IR spectra have been measured within several spectral regions from 360 to 4000 cm^{-1} and at different pyrolytic temperatures ranging from 500 to 1150 °C.

Gas-phase spectra of the primary pyrolysis products were recorded with a resolution of 1 cm^{-1} in the 600 to 4000 cm^{-1} region at a pyrolytic temperature of 700 °C, when the precursor **2** has almost completely been decomposed. Owing to the low pressure (2.5 Pa) and the comparatively low pyrolytic temperature (700 °C) employed in these experiments, intermolecular reactions were suppressed and the gas-phase IR spectrum of the intermediate **3** together with that of the byproduct 2-methylpropene[37] was obtained. The bands assigned to gaseous **3** are summarized in Table 2.

The analysis of IR spectra of pyrolysis products obtained at 1150 °C confirmed our mass spectroscopic results. The main products of the low-pressure pyrolysis of **2** are in fact H_2O, S_2O,[38] SO_2,[39] and 2-methylpropene.[37] In addition to these, traces of several hydrocarbons, produced by thermal decomposition of 2-methylpropene (CH_4,[40] 1,2-propadiene (C_3H_4),[41] propyne (C_3H_4),[42] and ethyne (C_2H_2)[43]) were also identified in the final gaseous pyrolysis products by comparison with reference spectra. Apart from H_2O and 2-methylpropene, these molecules were not obtained in the matrix isolation experiments because they are not formed by unimolecular decomposition pathways.

Owing to a comparatively large amount of supplementary pyrolysis products formed at 1150 °C as well as the low abundance of transient HSOH (**1**) in the gaseous pyrolysis products, the assignment of spectral features from (**1**) in the 600 to 1400 cm^{-1} region turned out to be difficult. At least the three fundamental bands of **1**, expected in this spectral region (Table 1), were found to interfere strongly with bands of several supplementary pyrolysis products (i.e., S_2O[38] and accompanying hydrocarbons[37,43]).

The difficulties arising in the 400–1400 cm^{-1} spectral range have been obviated by recording IR spectra in the regions of the characteristic O–H and S–H stretching fundamentals of **1**. Figures 8 and 9 illustrate the spectral regions

at $\approx$3600 and $\approx$2550 cm^{-1}, respectively, recorded with an effective resolution of 0.011 cm^{-1}. Although it is located in a region where strong transitions of gaseous water occur, the O–H stretching band of **1**, centered at 3626 cm^{-1}, is clearly visible in Figure 8. A full analysis of the rotational structure of these IR bands will be reported elsewhere. Nevertheless, for the unequivocal gas-phase IR detection of **1** it is possible to obtain a sufficient amount of information from the envelope of the two stretching fundamentals shown in Figures 8 and 9.

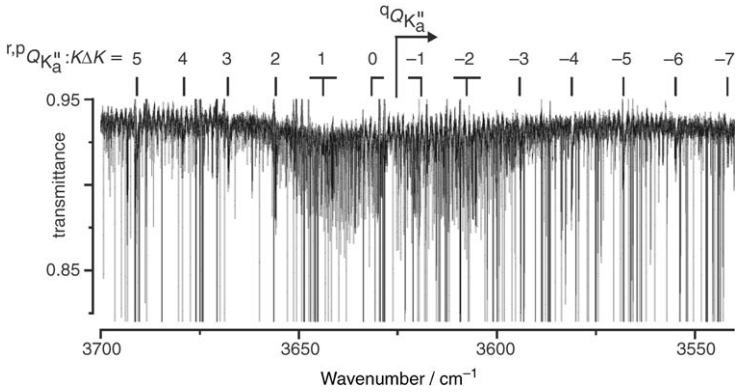

Figure 8. Survey IR spectrum of the O–H stretch of HSOH (**1**) (centered at $\tilde{\nu}$ = 3625.6 cm^{-1}) obtained by low-pressure pyrolysis of tBu$_2$SO (**2**); effective resolution 0.011 cm^{-1}. $^{p}Q_7$ to $^{r}Q_5$ branches of the *c*-type band and some *a*-type $^{q}Q_{K_a}$ branches at the band center are indicated. Major absorptions are attributed to the byproduct H_2O.

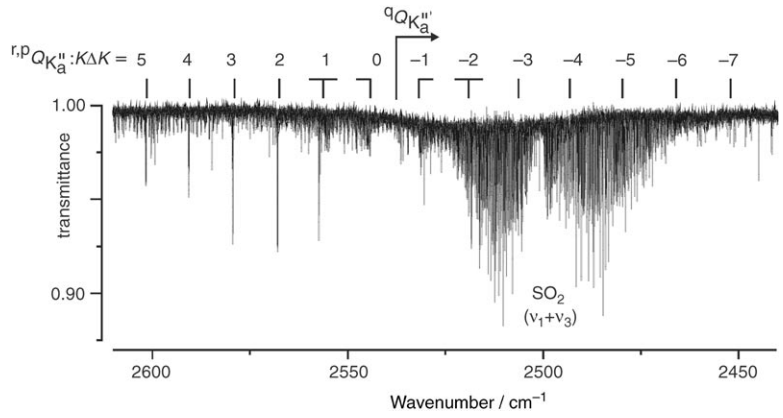

Figure 9. Survey IR spectrum of the S–H stretch of HSOH (**1**) (centered at 2538 cm^{-1}) and the (ν_1+ν_3) combination band of the byproduct SO_2 (centered at 2500 cm^{-1}) obtained by low-pressure pyrolysis of tBu$_2$SO (**2**); effective resolution 0.011 cm^{-1}. $^{p}Q_7$ to $^{r}Q_5$ branches of the *b*-type band and some *a*-type $^{q}Q_{K_a}$ branches are indicated.

Gas-phase IR bands of HSOH (1): The HSOH molecule is an asymmetric rotor with a much larger rotational constant A (6.7403 cm^{-1}) than B (0.5097 cm^{-1}) and C (0.4950 cm^{-1}).[4] From the nearly right-angular structure of the HSOH molecule,[4] it can be ascertained that both the O–H and S–H vibrations should exhibit some characteristics of perpendicular bands because the dipole moment associated with these two fundamentals changes along directions perpendicular to the principal axis a that almost coincides with the S–O bond vector. Indeed, these two stretching vibrations strongly resemble a perpendicular band of a slightly asymmetric prolate rotor ($\kappa = (2B-A-C)/(A-C) = -0.995$, Figures 8 and 9). The wings of these bands are dominated by $^{r,p}Q_K$ branches separated approximately by $\Delta\tilde{\nu} \cong (2A-B-C) \cong 12.5$ cm^{-1}.

$^{r,p}Q_{K_a}$ branches in the high and low wavenumber wings of the O–H stretch are denoted in Figure 8 up to $K_a'' = 5$ ($\Delta K = +1$) and 7 ($\Delta K = -1$), respectively. Fitting the observed $^{r,p}Q_{K_a}$ branch wavenumbers for $K_a'' = 3$ to 6 to Equation (7)[44] furnishes an approximate value for the difference between the ground state rotational constants $(2A''-B''-C'')$ of 12.47 ± 0.04 cm^{-1}, which is in perfect agreement with the value reported from a previous microwave spectroscopic investigation (12.4758 cm^{-1})[4] and is a simple but conclusive proof of the correct assignment of the observed vibrational band.

$$(2A''-B''-C'') \cong \frac{^{r}Q_{K-1} - {}^{p}Q_{K+1}}{2K_a} \qquad (7)$$

Because the HSOH molecule does not possess a symmetry axis or a symmetry plane, the change in the dipole moment accompanying the O–H stretch has components along at least two principal axes, resulting in a *a*/*c* hybrid band with both a parallel and a perpendicular component. Parallel (*a* type) band transitions are most easily detected near the band center, where some weak ^{q}Q branches are spread out to lower wavenumbers (Figure 8), indicating a negative sign of the difference of the respective vibration–rotation constants $(\alpha^A - \alpha^B)$, where $\alpha^A = A''-A'$ and $\alpha^B = B''-B'$.

The S–H stretch of **1** is found slightly above the (ν_1+ν_3) combination band of the byproduct SO_2, centered at 2500.0 cm^{-1} (Figure 9). Although the S–H stretch is by far the weakest fundamental detected in the matrix spectra, some regularly spaced, strong features spread out from the band centre at 2538 cm^{-1} to higher wavenumbers, which were tentatively assigned to $^{r}Q_{K_a}$ branches of the perpendicular component of the S–H stretch (denoted in Figure 9 up to $K\Delta K = 5$). Unfortunately, the low wavenumber wing of this band is buried under the (ν_1+ν_3) combination band of SO_2. The corresponding $^{p}Q_{K_a}$ branches, denoted in Figure 9 up to $K\Delta K = -7$, are, however, discernible at on the expanded scale of the experimental spectra. Again, the assignment of this vibrational band may be proved by fitting the observed $^{r,p}Q_{K_a}$

branch wavenumbers to Equation (7), where $K_a'' = 3$–6, to furnish the approximate value $(2A''-B''-C'') \cong 12.46 \pm 0.05\ cm^{-1}$.

The perpendicular band associated with the S–H stretch of **1** reveals an *a*/*b* hybrid band rather than an *a*/*c* hybrid. Thus, the dipole moment accompanying this vibration changes along both the intermediate and the smallest inertial axes, as one would expect from the nearly right-angular structure of the HSOH molecule. The effect of asymmetry on type *b* bands is to produce a depletion of intensity near the band centre (a band gap). Hence the comparatively strong central $^{r}Q_0$ and $^{P}Q_1$ branches are degraded away from the central gap. The $^{q}Q_K$ branches of the parallel component of this hybrid band are easily discernible in Figure 9 near the band center. They spread out to lower wavenumbers.

Thermochemistry of *t*BuSOH (3) and HSOH (1)

The low abundance of thermally stable **1** in the final thermolysis products of the pyrolysis reaction compared to large amounts of H_2O is an intriguing result from our spectroscopic investigations. Matrix-isolation experiments have provided compelling evidence that both **1** and H_2O are furnished by the pyrolysis reaction of **3** through competing unimolecular decomposition pathways [Eq. (8)]. Indeed, our computational study of the thermal decomposition routes of **3** renders the formation of **1** and H_2OS (**4**) possible (Figures 4, 5). Compound **4** is assumed to decompose rapidly into either H_2O and S(^{1}D) or **1** at pyrolytic temperatures. On the other hand, **1** may rearrange into **4**, which subsequently decomposes to water and elemental sulfur.

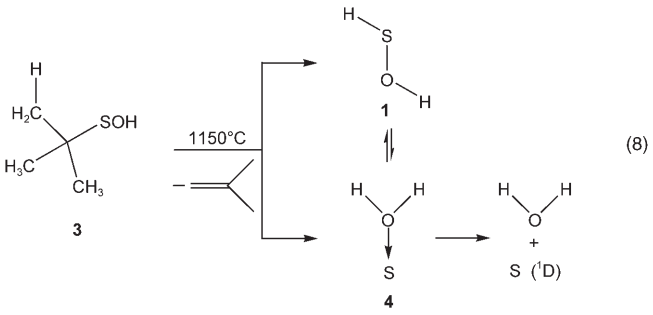

(8)

In order to generate H_2O by unimolecular decomposition reactions from **3**, reactive sulfur atoms should also be released. It should be mentioned that **4** is predicted[8b] to be thermodynamically unstable with respect to $H_2O + S(^3P)$, but this dissociation is spin forbidden, and may be slow compared to the discussed decomposition into $H_2O + S(^1D)$ [Eq. (8)]). Although formation of sulfur atoms has not been observed spectroscopically, their presence in the pyrolysis products is indicated by the mass spectra of the final pyrolysis products. The strongest signals attributed to sulfur-containing species in these spectra are attributed to the molecular ions $[S]^{+\cdot}$ (m/z 32) and $[H_2S]^{+\cdot}$ (m/z 34).

In general, two different unimolecular thermal decomposition routes of **1** may be considered [Eq. (9)]. Both routes are initiated by hydrogen migration, generating either H_2OS (**4**) or H_2SO (**4a**). However, only the first route, yielding H_2O and sulfur as final products, has been established by matrix isolation experiments, while the second route leading to H_2 and SO [Eq. (10)] is excluded, since the latter molecule has not been observed in the matrix-isolated products.

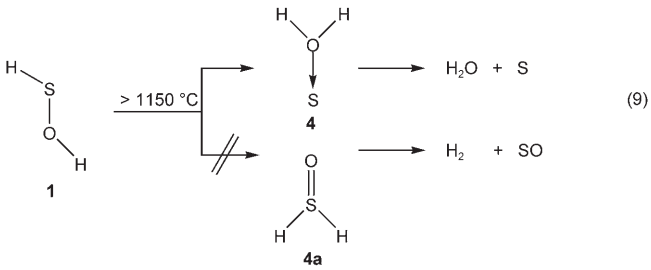

(9)

Our experimental results are also in good agreement with a recent computational study at the QCISD(T)/6-311+G-(3df,2p) level of theory.[8b] According to these calculations, **1** is predicted to be more stable at 0 K than its isomers **4** and **4a** by 166 and 73 kJ mol^{-1}, respectively, and separated from them by activation barriers of 205 and 241 kJ mol^{-1}, respectively. Thus, the relatively high thermal stability with respect to gas-phase unimolecular decomposition observed for **1** may be attributed to a high kinetic barrier to hydrogen migration, although, at this level of theory, isomerization to **4** is clearly favored.

In addition to unimolecular decomposition routes of both **3** and **1**, several competing intermolecular processes releasing S_2O have been established by mass spectrometry and gas-phase IR spectroscopy. Among these are condensation reactions of **3** [Eq. (4)] and **1**. The intermediate **5** formed in the pyrolysis zone will deliver S_2O and HSSOH (**6**) [Eq. (5)].

Furthermore, excited singlet sulfur atoms, generated along with H_2O by unimolecular processes, may also react with **3** to yield transient *tert*-butylthiosulfoxylic acid, *t*BuSSOH (**7**) [Eq. (10)], which is thermodynamically more stable than the branched isomer *t*BuS(O)SH that bears a sulfoxide group.[14a] It has recently been shown to be an intermediate of the flash pyrolysis of *t*BuS(O)S*t*Bu (**5**), and has been characterized by its gas-phase IR spectrum.[14a]

Thus, several intermolecular reactions are competing in the pyrolysis zone to yield S_2O and HSSOH (**6**) in experiments carried out at higher pressures without a carrier gas.

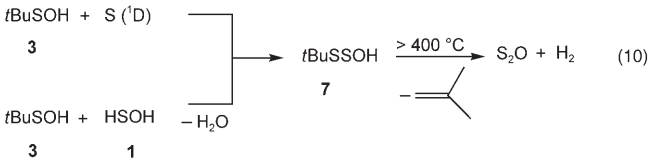

(10)

Conclusions

Elusive sulfenic acid, HSOH (**1**), has been synthesized by low-pressure pyrolysis of *t*Bu_2SO (**2**) according to Equation (1), and conclusively characterized by both matrix-IR and gas-phase IR spectroscopy. To the best of our knowledge, the parent sulfenic acid **1** is hitherto the first member of any sulfenyl derivative containing a reactive S–H moiety that has unequivocally been characterized by its gas-phase IR spectrum.

The mechanism of formation of **1** by flash pyrolysis of **2** has been studied by quantum chemical calculations, and different pyrolysis experiments monitored by mass spectrometry as well as by matrix and gas-phase IR spectroscopy. In agreement with theoretical and experimental results, **1** appears to be formed through several successive unimolecular steps via the primary decomposition product *t*BuSOH (**3**). Contrary to previous reports,[14b] but in agreement with the results of our quantum chemical calculations, no evidence has been found for the formation of the elusive S-protonated isomer *t*Bu(H)SO (**3a**). The intermediate **3** may decompose by two competing intramolecular reactions according to Equation (8) forming **1** or its energetically least stable isomer H_2OS (**4**). The latter may either reversibly rearrange into **1** or decompose into H_2O and most probably $S(^1D)$. The reversible rearrangement between **1** and **4** also opens a unimolecular decomposition channel for **1**.

Higher pressures and prolonged residence times in the pyrolysis zone allow competitive bimolecular decomposition routes of **3** leading to HSSOH (**6**) and S_2O as the major products.

Experimental Section

Quantum chemical calculations: Quantum chemical calculations have been performed with the following program packages; ACES II[45] (Coupled-cluster calculations), TURBOMOLE[46] (DFT and RI-MP2 calculations), as well as GAUSSIAN 03[47] and GAUSSIAN 98[48] (DFT and MP2 calculations).

Di-*tert*-butylsulfoxide, *t*Bu_2SO (2): The starting compound **2** was prepared by selective oxidation of di-*tert*-butyl sulfide with a mixture of H_2O_2 and selenium dioxide as described by Drabowicz and Mikolajczyk.[49]

Mass spectra: The starting compound, **2**, was stored at its own vapor pressure at ambient temperature in a 50 mL glass flask. As shown in Figure 10, this storage flask was connected to the pyrolysis tube (quartz glass, inner diameter 12 mm, length 200 mm) via an inlet valve. The pyrolysis tube was heated by an oven with a thermocouple temperature controller (Heraeus). The products were fed from the pyrolysis tube into a vacuum cell composed of Pyrex tubes (inner diameter 0.1 m, volume: 0.027 m^3), which were evacuated by a turbomolecular pump equipped with cold traps and a rotary vane pump as a roughing pump. The measurements were carried out under flow conditions (500–900 mg **2** per h) at a pressure of 0.1 Pa, which was adjusted by means of the inlet valve and the outlet valve connecting the cell to the vacuum system. Under these conditions (the mean residence time of a molecule in the cell was estimated to be ≈1 s), the large volume of the cell did not have a negative influence on the fraction of HSOH (**1**) in the pyrolysis products.

The mass spectra have been recorded with a residual gas analyzer system (LM 70, Leda-Mass Ltd.) consisting of an enclosed electron-ionization ion source, a quadrupole analyzer 300D and a channel-plate detector. The mass spectrometer was connected to the cell by a gate valve and an aperture plate (hole diameter 300 μm) that controlled the gas inlet. At the operating pressure of 0.1 Pa in the cell, the pressure inside the mass spectrometer was 0.0005 Pa.

Matrix isolation: *t*Bu_2SO (**2**) was placed into a small U trap that was mounted in front of the matrix support (a metal mirror) and cooled to 0 °C. A stream of argon gas was passed over the sample in the U trap, and the resulting mixtures of gaseous **2** and argon (≈1:1000), were forced through a pipe with a corundum (Al_2O_3) nozzle (1 mm i.d.), that was heated over a length of ≈10 mm with a platinum wire (0.25 mm o.d.), prior to deposition on the matrix support at ≈15 K. Details of the matrix apparatus have been described elsewhere.[50]

Matrix IR spectra of the deposits were recorded on a Bruker IFS66v FT instrument in the reflectance mode with a transfer optic. The interferometer was equipped with a globar source, a KBr beam splitter, and a DTGS detector; 64 scans with an apodized resolution of 0.5 cm^{-1} were collected for each spectrum over the 400–4000 cm^{-1} region. A total of 16 matrices with different pyrolytic temperatures were prepared and investigated. IR spectra of the deposits prepared from gaseous mixtures of 2-methylpropene and argon (1:1000) and H_2O/Ar mixtures with varying amounts of water were also recorded and used as reference spectra.

Gas-phase IR spectra: The quartz tube oven used in the gas-phase experiments was attached to a spherical (o.d. 30 cm) multipath cell with a total path length adjusted to 40 m. This cell was equipped with KBr windows and argon-flushed mirrors (f = 50 cm) in a White-type setup. It was connected to the internal detector chamber of a Bruker 120 HR FT spectrometer by changing the f number of the internal spectrometer beam from 6 (as provided by the Bruker optics) to 20 by mean of transfer optics placed in the sample chamber of the spectrometer. The mirrors of the White cell were flushed with argon introduced at a pressure adjusted to 20 Pa, while the cell was evacuated by a two-stage rotary pump (65 m^3h^{-1}) and a liquid-nitrogen cold trap placed at right angles to the

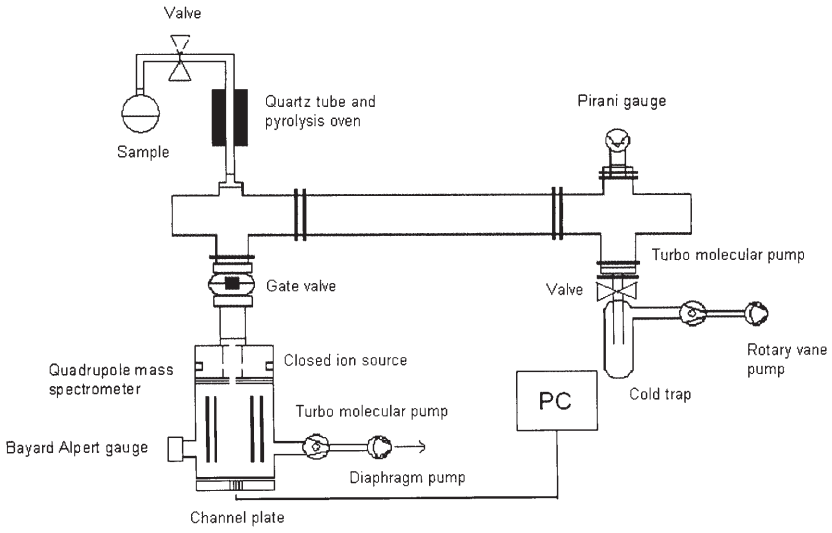

Figure 10. Low-pressure flash pyrolysis set-up with mass spectrometer.

gas inlet. The progress of the thermolysis was simultaneously monitored by IR spectroscopy and mass spectrometry with the above-mentioned mass spectrometer. The mass spectrometer was attached between the multipath cell and the pump system, and separated from the line by a hole-shaped skimmer (0.5 mm i.d.) mounted in front of the ion source to prevent the pressure exceeding the operating pressure in the quadrupole analyzer.

Gas-phase IR spectra were recorded on pyrolysed mixtures of gaseous **2** in Ar. Gaseous Ar was passed over **2** placed in a Schlenk tube that was attached to the quartz tube oven. The sample was slowly heated from 60 to 80 °C. The total pressure in the multipath cell was adjusted to $\approx$90 Pa and the thermolysis was carried out at 1200 °C. Data points were collected at a rate of 40 kHz over four spectral regions: 380–825 cm^{-1}, 600–1400 cm^{-1}, 2000–2900 cm^{-1}, and 1800–3850 cm^{-1}.

The Bruker 120 HR interferometer was equipped with a 100 W tungsten halogen source and an InSb detector for the region $>$1800 cm^{-1}. In the 1800–3900 cm^{-1} range (O–H stretch and S–H stretch), a KBr beam splitter was employed and a total of 46 scans were co-added at a resolution of 0.011 cm^{-1}. The S–H stretch of HSOH was studied with a CaF_2 beam splitter and an optical wide-band pass filter to eliminate radiation outside the spectral region from 2000–2900 cm^{-1}. A total of 20 scans with an instrumental resolution of 0.011 cm^{-1} were collected.

For the 600–1400 cm^{-1} range, the interferometer was equipped with a globar source, a KBr beam splitter, and a MCT 600 detector. An optical filter was used to eliminate radiation $>$1400 cm^{-1} and 25 scans were collected at a resolution adjusted to 0.016 cm^{-1}. Measurements in the 380–825 cm^{-1} range were carried out with a globar source, a liquid-He-cooled Cu/Ge detector and a 3.5 μm Mylar beam splitter.

Acknowledgements

We thank Prof. Dr. H. Bürger for many valuable suggestions, Dr. S. v. Ahsen and Mr. F. Lücker for assistance in the matrix isolation and gas-phase experiments, respectively. Financial support by the Deutsche Forschungsgemeinschaft (some of us are supported within the SFB 494) and the Fonds der Chemischen Industrie is gratefully acknowledged.

[1] a) H. Offermanns, G. H. Dittrich, N. Steiner, *Chem. Unserer Zeit* **2000**, *34*, 150–159; b) M. Petterson, S. Tuominen, M. Räsänen, *J. Phys. Chem. A* **1997**, *101*, 1166–1171; c) R. L. Redington, W. B. Olsen, P. C. Cross, *J. Chem. Phys.* **1962**, *36*, 1311–1326.

[2] a) R. Steudel, *Angew. Chem.* **1975**, *87*, 683–692; *Angew. Chem. Int. Ed. Engl.* **1975**, *14*, 655–664; b) E. Isoniemi, L. Khriachtchev, M. Petterson, M. Räsänen, *J. Phys. Lett.* **1999**, *311*, 47–54; c) S. Urban, J. Behrend, K. M. T. Yamada, G. Winnewisser, *J. Mol. Spectrosc.* **1996**, *177*, 280–284.

[3] a) L. Wang, J. Zhang, *THEOCHEM* **2002**, *581*, 129–138; b) A. H. Otto, R. Steudel, *Eur. J. Inorg. Chem.* **2000**, 617–624; c) D. Laakso, P. Marshall, *J. Phys. Chem.* **1992**, *96*, 2471–2474.

[4] G. Winnewisser, F. Leven, S. Thorwirth, M. Behnke, J. Hahn, J. Gauss, E. Herbst, *Chem. Eur. J.* **2003**, *9*, 5501–5510.

[5] a) G. S. Tyndal, A. R. Ravishankara, *Int. J. Chem. Kinet.* **1991**, *23*, 483–527; b) W. B. DeMore, S. P. Sander, D. M. Golden, R. F. Hampson, M. J. Kurylo, C. J. Howard, A. R. Ravishankara, C. E. Kolb, M. J. Molina, *Chemical Kinetics and Photochemical Data for Use in Stratospheric Modeling* (Evaluation Number 10), JPL, Pasadena, **1992**, Publication No. 92–20; c) R. Atkinson, D. L. Baulch, R. A. Cox, R. F. Hampson, Jr., J. A. Kerr, J. Troe, *J. Phys. Chem. Ref. Data* **1992**, *21*, 1125–1568.

[6] Combustion chemistry of sulfur: M. Frenklach, J. H. Lee, J. N. White, W. C. Gardiner, Jr., *Combust. Flame* **1981**, *41*, 1–16.

[7] a) D. L. Singleton, R. J. Cvetanoviæ, *J. Phys. Chem. Ref. Data* **1988**, *17*, 1377–1437; b) N. Balucani, P. Casavecchia, D. Stranges, G. G. Volpi, *Chem. Phys. Lett.* **1993**, *211*, 469–472.

[8] a) S. Wolfe, H. B. Schlegel, *Gazz. Chim. Ital.* **1990**, *120*, 285–290; b) A. Goumri, J.-D. R. Rocha, D. Laakso, C. E. Smith, P. Marshall, *J. Chem. Phys.* **1994**, *101*, 9405–9411; c) A. Goumri, D. Laakso, J.-D. R. Rocha, C. E. Smith, P. Marshall, *J. Chem. Phys.* **1995**, *102*, 161–169.

[9] R. R. Smardzewski, M. C. Lin, *J. Chem. Phys.* **1977**, *66*, 3197–3204.

[10] M. Iraqi, H. Schwarz, *Chem. Phys. Lett.* **1994**, *221*, 359–362.

[11] a) N. P. Machara, S. B. Ault, *J. Mol. Struct.* **1988**, *172*, 129–138; b) T. D. Crawford, N. A. Burton, H. F. Schaefer, III, *J. Chem. Phys.* **1992**, *96*, 2044–2047; c) L. Andrews, T. C. McInnis, Y. Hannachi, *J. Chem. Phys.* **1992**, *96*, 4248–4254.

[12] a) U. P. Agarwal, A. J. Barnes, W. J. Orville-Thomas, *Can. J. Chem.* **1985**, *63*, 1705–1707; b) E. Jurg, C. Wei-Chen, Y. Chin-Hui, L. Yuan-Pern, C. Bing-Ming, *J. Chem. Phys.* **1998**, *108*, 6197–6204.

[13] Review: P. De Maria, *The Chemistry of Sulfenic Acids and their Derivatives* (Ed.: S. Patai), Wiley, New York, **1990**, p. 293.

[14] a) A. Königshofen, M. Behnke, M. Hoverath, J. Hahn, *Z. Anorg. Allg. Chem.* **1999**, *625*, 1778–1786; b) F. A. Davis, R. L. Billmers, *J. Org. Chem.* **1985**, *50*, 2593–2595.

[15] C. Møller, M. S. Plesset, *Phys. Rev.* **1934**, *46*, 618–622.

[16] R. G. Parr, W. Yang, *Density Functional Theory of Atoms and Molecules*, Academic Press, London, **1994**.

[17] A. D. Becke, *J. Chem. Phys.* **1993**, *98*, 5648–5652.

[18] a) R. Krishnan, J. S. Binkley, R. Seeger, J. A. Pople, *J. Chem. Phys.* **1980**, *72*, 650–654; b) A. D. McLean, G. S. Chandler, *J. Chem. Phys.* **1980**, *72*, 5639–5648.

[19] K. Eichkorn, O. Treutler, H. Öhm, M. Häser, R. Ahlrichs, *Chem. Phys. Lett.* **1995**, *242*, 652–660.

[20] F. Weigend, F. Furche, R. Ahlrichs, *J. Chem. Phys.* **2003**, *119*, 12753–12762.

[21] a) C. Gonzalez, H. B. Schlegel, *J. Chem. Phys.* **1989**, *90*, 2154–2161; b) C. Gonzalez, H. B. Schlegel, *J. Phys. Chem.* **1990**, *94*, 5523–5527.

[22] M. W. Chase, Jr., C. A. Davies, J. R. Downey, Jr., D. J. Frurip, R. A. McDonald, A. N. Syverud, *J. Phys. Chem. Ref. Data* **1985**, *14*, 1211, 1248, 1274, 1280, 1290.

[23] K. Raghavachari, G. W. Trucks, J. A. Pople, M. Head-Gordon, *Chem. Phys. Lett.* **1989**, *157*, 479–483.

[24] J. Gauss, J. F. Stanton, *Chem. Phys. Lett.* **1997**, *276*, 70–77.

[25] T. H. Dunning, *J. Chem. Phys.* **1989**, *90*, 1007–1023.

[26] M. J. Frisch, J. A. Pople, J. S. Binkley, *J. Chem. Phys.* **1984**, *80*, 3265–3269.

[27] I. M. Mills, in *Molecular Spectroscopy: Modern Research* (Eds.: K. N. Rao, C. W. Matthews), Academic Press, New York, **1972**, p. 115.

[28] A scaling factor of 0.9614 has been determined originally for B3LYP/6-31G(d) (A. P. Scott, L. Radom, *J. Phys. Chem.* **1996**, *100*, 16502–16513), but also proves useful in the case of B3LYP/6-31G-(2d,p).

[29] a) P. W. Schenk, R. Z. Steudel, *Z. Anorg. Allg. Chem.* **1966**, *342*, 253–262; b) P. W. Schenk, *Z. Anorg. Allg. Chem.* **1941**, *248*, 297–312; c) E. Tiemann, J. Hoeft, F. J. Lovas, D. R. Johnson, *J. Chem. Phys.* **1974**, *60*, 5000–5004; d) J. Nakayama, S. Aoki, J. Takayama, A. Sakamato, Y. Sugihara, A. Ishii, *J. Am. Chem. Soc.* **2004**, *126*, 9085–9093.

[30] a) A. Engdahl, B. Nelander, *J. Mol. Struct.* **1989**, *193*, 101–109; b) D. Forney, M. E. Jacox, W. E. Thompson, *J. Mol. Spectrosc.* **1993**, *157*, 479–493; c) O. N. Ventura, K. Irving, Z. Latajka, *Chem. Phys. Lett.* **1994**, *217*, 436–442, and references therein; d) B. Nelander, *J. Mol. Struct.* **1990**, *222*, 121–126.

[31] A. Heckel, W. Pfleiderer, *Tetrahedron Lett.* **1983**, *24*, 5047–5050.

[32] M. Larzillière, M. E. Jacox, *J. Mol. Spectrosc.* **1980**, *79*, 132–150.

[33] P. N. Clough, B. A. Thrush, D. A. Ramsay, J. G. Stamper, *Chem. Phys. Lett.* **1973**, *23*, 155–156.

[34] a) M. Behnke, J. Hahn, unpublished results; b) A. Königshofen, *Dissertation*, Köln (Germany), **1997**, p. 70.

[35] a) I. Schwager, A. Arkell, *J. Am. Chem. Soc.* **1967**, *89*, 6006–6008; b) J. S. Wells, R. L. Sams, W. J. Lafferty, *J. Mol. Spectrosc.* **1979**, *77*, 349–364; c) M.-L. Juntilla, W. J. Lafferty, J. B. Burkholder, *J. Mol. Spectrosc.* **1994**, *164*, 583–585.

[36] A. G. Hopkins, C. W. Brown, *J. Chem. Phys.* **1975**, *62*, 2511–2512.
[37] a) T. Shimanouchi, *Tables of Molecular Vibrational Frequencies Consolidated Volume I*, National Bureau of Standards, **1972**, 1–160; b) W. Luettge, S. Braun, *Ber. Buns. Gesellschaft* **1967**, *71*, 34–40.
[38] a) W.-J. Lo, Y.-J. Wu, Y.-J. Lee, *J. Chem. Phys.* **2002**, *117*, 6655–6661; b) T. Muller, T. H. Vaccaro, F. Perez-Bernal, F. Iachello, *J. Chem. Phys.* **1999**, *111*, 5038–5055.
[39] a) R. J. Corice, K. Fox, G. D. T. Tejwani, *J. Chem. Phys.* **1973**, *58*, 265–270; b) A. S. Pine, P. F. Moulton, *J. Mol. Spectrosc.* **1977**, *64*, 15–30.
[40] J. P. Champion, J. C. Hilico, C. Wenger, *J. Mol. Spectrosc.* **1989**, *133*, 256–272.
[41] a) J. Chazelas, J. Plíva, A. Valentin, L. Henry, *J. Mol. Spectrosc.* **1985**, *110*, 326–338; b) F. Hegelund, H. Bürger, O. Polanz, *J. Mol. Spectrosc.* **1994**, *164*, 152–166.
[42] a) E. R. T. Kerstel, K. K. Lehmann, B. H. Pate, G. Scoles, *J. Chem. Phys.* **1994**, *100*, 2588–2595; b) K. Pekkala, *J. Mol. Spectrosc.* **1990**, *144*, 416–428.
[43] Y. Kabbadj, M. Herman, *J. Mol. Spectrosc.* **1991**, *150*, 535–565.
[44] a) G. Herzberg, *Molecular Spectra and Molecular Structure II, IR and Raman Spectra of Polyatomic Molecules*, Nostrand Reinhold, **1945**, Chapter IV, p. 435; b) X'' denotes the lower (vibrational ground) state and X' the upper (vibrational excited) state. X refers to rotational constants or quantum numbers, respectively.
[45] J. F. Stanton, J. Gauss, J. D. Watts, W. J. Lauderdale, R. J. Bartlett, *Int. J. Quantum Chem. Symp.* **1992**, *26*, 879–894.
[46] R. Ahlrichs, M. Bär, M. Häser, H. Horn, C. Kölmel, *Chem. Phys. Lett.* **1989**, *162*, 165–169.
[47] Gaussian 03, Revision C.02, M. J. Frisch, G. W. Trucks, H. B. Schlegel, G. E. Scuseria, M. A. Robb, J. R. Cheeseman, J. A. Montgomery, Jr., T. Vreven, K. N. Kudin, J. C. Burant, J. M. Millam, S. S. Iyengar, J. Tomasi, V. Barone, B. Mennucci, M. Cossi, G. Scalmani, N. Rega, G. A. Petersson, H. Nakatsuji, M. Hada, M. Ehara, K. Toyota, R. Fukuda, J. Hasegawa, M. Ishida, T. Nakajima, Y. Honda, O. Kitao, H. Nakai, M. Klene, X. Li, J. E. Knox, H. P. Hratchian, J. B. Cross, V. Bakken, C. Adamo, J. Jaramillo, R. Gomperts, R. E. Stratmann, O. Yazyev, A. J. Austin, R. Cammi, C. Pomelli, J. W. Ochterski, P. Y. Ayala, K. Morokuma, G. A. Voth, P. Salvador, J. J. Dannenberg, V. G. Zakrzewski, S. Dapprich, A. D. Daniels, M. C. Strain, O. Farkas, D. K. Malick, A. D. Rabuck, K. Raghavachari, J. B. Foresman, J. V. Ortiz, Q. Cui, A. G. Baboul, S. Clifford, J. Cioslowski, B. B. Stefanov, G. Liu, A. Liashenko, P. Piskorz, I. Komaromi, R. L. Martin, D. J. Fox, T. Keith, M. A. Al-Laham, C. Y. Peng, A. Nanayakkara, M. Challacombe, P. M. W. Gill, B. Johnson, W. Chen, M. W. Wong, C. Gonzalez, J. A. Pople, Gaussian, Inc., Wallingford CT, **2004**.
[48] Gaussian 98 (Revision A.11), M. J. Frisch, G. W. Trucks, H. B. Schlegel, G. E. Scuseria, M. A. Robb, J. R. Cheeseman, V. G. Zakrzewski, J. A. Montgomery, Jr., R. E. Stratmann, J. C. Burant, S. Dapprich, J. M. Millam, A. D. Daniels, K. N. Kudin, M. C. Strain, O. Farkas, J. Tomasi, V. Barone, M. Cossi, R. Cammi, B. Mennucci, C. Pomelli, C. Adamo, S. Clifford, J. Ochterski, G. A. Petersson, P. Y. Ayala, Q. Cui, K. Morokuma, P. Salvador, J. J. Dannenberg, D. K. Malick, A. D. Rabuck, K. Raghavachari, J. B. Foresman, J. Cioslowski, J. V. Ortiz, A. G. Baboul, B. B. Stefanov, G. Liu, A. Liashenko, P. Piskorz, I. Komaromi, R. Gomperts, R. L. Martin, D. J. Fox, T. Keith, M. A. Al-Laham, C. Y. Peng, A. Nanayakkara, M. Challacombe, P. M. W. Gill, B. Johnson, W. Chen, M. W. Wong, J. L. Andres, C. Gonzalez, M. Head-Gordon, E. S. Replogle, J. A. Pople, Gaussian, Inc., Pittsburgh PA, **2001**.
[49] J. Drabowicz, M. Mikolajczyk, *Synthesis* **1978**, 758–759.
[50] H. Schnöckel, H. Willner, in *IR and Raman Spectroscopy, Methods and Applications* (Ed.: B. Schrader), VCH Weinheim, **1994**, p. 297.

Received: January 28, 2005
Revised: June 16, 2005
Published online: October 20, 2005

